Selectively Production of Levoglucosenone from Cellulose via Catalytic Fast Pyrolysis

Qian Le
Guangzhou Institute of Energy Conversion
Liqun Jiang (lqjiang@ms.giec.ac.cn)
Guangzhou Institute of Energy Conversion https://orcid.org/0000-0002-8541-7539
Zengli Zhao
Guangzhou Institute of Energy Conversion

Research Article

Keywords: Levoglucosenone, Magnetic solid acid, Catalytic fast pyrolysis, Cellulose

Posted Date: March 12th, 2021

DOI: https://doi.org/10.21203/rs.3.rs-280794/v1

Selectively production of levoglucosenone from cellulose via catalytic fast pyrolysis

Le Qian[a,b], Liqun Jiang[a,*], Zengli Zhao[a]

[a]*CAS Key Laboratory of Renewable Energy, Guangdong Provincial Key Laboratory of New and Renewable Energy Research and Development, Guangzhou Institute of Energy Conversion, Chinese Academy of Sciences, Guangzhou 510640, China*

[b]*Nano Science and Technology Institute, University of Science and Technology of China, Suzhou 215000, China*

**Corresponding author: Tel: +86-020-87057721 Fax: +86-020-87057737*

E-mail: lqjiang@ms.giec.ac.cn

Abstract

Levoglucosenone (LGO) has a wide range of utilization in the field of organic synthesis. Magnetic solid acid (Fe_3O_4/C-SO_3H_{600}) was used in fast pyrolysis of cellulose to produce LGO. It was demonstrated that the catalyst could promote the pyrolysis of cellulose to produce LGO, but the yield was affected by the pyrolysis temperature and the relative amount of catalyst. The yield of LGO reached 20.0 wt% from catalytic fast pyrolysis of cellulose at 300 °C, which was significantly higher than that from cellulose (0.3 wt%). Furthermore, the kinetic analysis and recycling results showed that the catalyst could not only reduce the required temperature of cellulose in fast pyrolysis, but also still efficiently promote the production of LGO after recovery and activation.

Key words: Levoglucosenone, Magnetic solid acid, Catalytic fast pyrolysis, Cellulose.

Introduction

A great interest burgeons in renewable biomass as a source for fuel and chemicals production for the demands to replace alternatives to fossil fuels (Jiang *et al.,* 2020a). Fast pyrolysis, one of the feasible and effective biomass utilization technology, can convert biomass into bio-oil (Sharifzadeh *et al.,* 2019; Zhang *et al.,* 2020). Bio-oil is a complex mixture of water and hundreds of organics including acids, ketones, aldehydes, esters, alcohols, furans, anhydrosugars, phenols and other macromolecular oligomers. Because of containing various compounds and the potential for wide range applications, it can be used as a liquid fuel or extracted valuable chemicals (Tshikesho *et al.,* 2019). However, the concentration of most components in bio-oil obtained from the traditional pyrolysis process is relatively low, and it is currently uneconomical to separate special compounds from bio-oil. There is no doubt that bio-oil production with a high content of target products is essential (Meng *et al.,* 2016). Recently, various selective pyrolysis methods have been investigated, such as pretreatment of raw material before pyrolysis, catalytic pyrolysis of biomass, and optimization of pyrolysis conditions (Zhang *et al.,* 2021; Jiang *et al.,* 2020b; Usino *et al.,* 2020).

Levoglucosenone (LGO) is an anhydrosugar with a unique structure, which includes not only six different functionalized carbon atoms, but also two chiral centers, containing α,β-unsaturated ketones and protected aldehyde functional groups. These unique properties make it a chiral synthon for the synthesis of a variety of new and valuable compounds, such as high-value drugs and bio-based polar aprotic solvent (Cao *et al.,* 2015; Zhang *et al.,* 2018; Liu *et al.,* 2020). Although LGO has a considerable value for use, the content of LGO in bio-oil obtained by conventional pyrolysis of cellulose is extremely low, hindering its further utilizations. Therefore, it

is essential to develop a suitable catalyst for cellulosic fast pyrolysis to achieve LGO with high yields. It has been proposed that the catalysts currently used in the cellulosic pyrolysis to produce LGO include ionic liquids, liquid inorganic acids and solid acids (Doroshenko *et al.,* 2019). Although ionic liquids can increase the yield of LGO significantly, high expenses make them unavailable in large-scale applications (Kudo *et al.,* 2017). Cellulose impregnated with liquid inorganic acids (*e.g.* phosphoric acid, sulfuric acid) is also performed to promote LGO production (Dobele *et al.,* 1999). However, this process shows several shortcomings: the impregnation of cellulose and acid requires a complicated pretreatment process; a large amount of waste acid is produced after the impregnation, which cannot be recycled and reused. In contrast, solid acid is thermally stable and can be readily recovered after pyrolysis. There is no need to go through a complicated impregnation process and only simple mechanical mixing with the cellulose is required. Therefore, solid acid is a better choice for catalytic fast pyrolysis of cellulose. Solid superacid SO_4^{2-}/ZrO_2 was subjected to catalytic pyrolysis, giving a LGO yield of 8.2 wt% (Wang *et al.,* 2011). Lu *et al.* (2014a) developed a superacid SO_4^{2-}/TiO_2-Fe_3O_4 for catalytic pyrolysis of cellulose at 300 °C, obtaining a LGO yield up to 15.4 wt%. Phosphoric acid-activated carbon catalyzed pyrolysis of cellulose greatly improved the yield of LGO (Ye *et al.,* 2017). The yield of LGO produced from cellulose catalyzed by solid acid still needs to be improved.

Based on previous research, an important and indispensable step for cellulose pyrolysis to generate LGO was the dehydration reaction (Zhang *et al.,* 2017). Regarding this procedure, it has been reported that both Fe_3O_4 and acid catalyst could enhance the dehydration behavior and promote the yield of LGO in catalytic fast pyrolysis cellulose (Lu *et al.,* 2014a; Halpern *et al.,* 1973). In this study, magnetic

solid acid Fe_3O_4/C-SO_3H_{600} was synthesized and applied in catalytic fast pyrolysis of cellulose to produce LGO. Different from previous reported investigations, this research could not only efficiently promote the conversion of cellulose to LGO, but also analyzed its kinetics and reaction mechanism in detail, and investigated the recovery and reuse performance of the catalyst.

Materials and methods

Materials

The microcrystalline cellulose, nano-Fe_3O_4 (≥99.5%, 20 nm) and glucose used in the experiment were purchased from Macklin biochemical Co., Ltd. (Shanghai). H_2SO_4 (99.8%) was purchased from Guangshi Agent Technology Co., Ltd. (Guangdong). Levoglucosan (LG) (>96%) and LGO (>96%) were purchased from Sigma-Aldrich (Shanghai).

Catalyst preparation

The preparation of the catalyst required two steps: carbonization and sulfonation. Firstly, the nano-Fe_3O_4 (2 g) and glucose (15 g) were mixed in deionized water (100 mL), and evaporated the water in an oil bath (100 °C) with vigorous stirring to ensure uniform dispersion of the nano-Fe_3O_4. After evaporation, the mixture was transferred to a crucible and heated to 500-700°C for a period of time in a tube furnace under N_2 atmosphere (240 mL/min) at a heating rate of 6 °C/min. The carbonized solid C/Fe_3O_4 therein was taken out and ground through a 200-mesh sieve, and then mixed with 98% H_2SO_4 at a ratio of 1 g/10 mL. After sulfonated in an oil bath for 20 h at a temperature of 150 °C, the sulfonated catalyst was washed with deionized water until neutral and dried at 105 °C for 24 h in an oven finally. The catalysts prepared at 500 °C, 600 °C and 700 °C were entitled Fe_3O_4/C-SO_3H_{500}, Fe_3O_4/C-SO_3H_{600} and Fe_3O_4/C-SO_3H_{700}, respectively.

Catalyst characterization

The X-ray diffraction analysis of the catalyst was carried out in an X'Pert PRO MPD X-ray diffractometer using Cu Kα radiation source (λ=0.15418 nm). Fourier transform infrared spectroscopy (FTIR, Bruker TENSOR27, Optik Instruments, Brno, Czech Republic) was used to analyze the functional groups contained in the catalyst. Scanning electron microscope (SEM, ZEISS EVO LS10, Cambridge, UK) was used to scan the surface morphology of the catalyst. The acid sites of the catalyst were determined by NH_3 temperature programmed desorption (NH_3-TPD, Chemisorption analyzer, Quantachrome Instruments, Boynton Beach, FL). Thermogravimetric experiment was carried out in a TG analyzer (SDT650, TA, USA). Sample was put into alumina crucible, and heated from 50 °C to 650 °C at the rate of 10, 20 and 40 °C/min.

Kinetic analysis

The kinetic parameters were obtained by distributed activation energy model (DAEM). It assumed that the thermal decomposition reaction consisted of many simple reactions that obeyed a normal distribution *f(E)*.

$$f(E) \sim N(E,\sigma) \tag{1}$$

Due to the existence of the kinetic compensation effect, the activation energy, the pre-reference factor, and the mechanism function were related to each other. Assuming that the pre-reference factor was a constant, the activation energy was only related to the mechanism function, as shown in formula (2).

$$\alpha = 1 - \int_0^{\infty} \exp\left[-\frac{A}{\beta} \Psi(E,T) \right] f(E) dE \tag{2}$$

where α is the conversion rate, %; β is the heating rate, °C/min; E is the activation energy, kJ/mol; A is the pre-exponential factor, s^{-1}; $\Psi(E, T)$ is the

temperature integral:

$$\Psi(E,T) = \int_0^T \exp\left(\frac{-E}{RT}\right) dT \tag{3}$$

Fast pyrolysis

The sample was subjected to fast pyrolysis in a semi-batch CDS reactor (CDS 5200, Oxford, PA, USA), and then the composition of the volatile products after pyrolysis was examined by Gas Chromatograph-Mass Spectrometer (GC-MS) (Agilent 7890A/5975C, Santa Clara, CA, USA). The sample was weighted and placed in the middle of the quartz tube, and both sides of the quartz tube were blocked with quartz wool. The sample was pyrolyzed at 250-500 °C for 20 s. The injector temperature was 280 °C, and the helium gas (1 mL/min) was used as carrier gas with a split ratio of 1:100. The capillary column used for chromatographic separation was Agilent HP-INNO (30 mm × 0.25 mm × 0.25 μm). The oven program was held at 40 °C for 3 min, then ramped to 280 °C at 5 °C/min and held at 280 °C for 8 min. The mass spectrometer operated at 70 eV in EI mode. After fast pyrolysis, the catalyst was recovered by the permanent magnet, and the recovered catalyst was subjected to Py-GC/MS experiment to verify its cyclic activity. The chromatographic peaks were identified by the NIST mass spectral data library. The quantification of products was performed by external standard method. Each experiment was performed in triplicate to ensure its repeatability. The yield and relative content of products were calculated as follows:

$$\text{Compound yield}\ (\text{wt}\%) = \frac{\text{mass of compound}}{\text{mass of cellulose}} \times 100\% \tag{4}$$

$$\text{Relative content of compound}\ (\%) = \frac{\text{Area of a compound}}{\text{Area of all compouds}} \times 100\% \tag{5}$$

Results and discussion

Catalyst characterization

The SEM images of the catalysts are shown in Fig. 1. It could be seen that the surface of Fe_3O_4/C-SO_3H_{500} and Fe_3O_4/C-SO_3H_{600} contained countless pores. This facilitated the contact of the catalysts with cellulose. Although there were many pores on the surface of Fe_3O_4/C-SO_3H_{700}, it was very messy, probably due to the excessive temperature destroying the pore structure on the surface of Fe_3O_4/C-SO_3H_{700}. Among the three catalysts, the surface area of Fe_3O_4/C-SO_3H_{500} (1.8 m^2/g) was larger than that of Fe_3O_4/C-SO_3H_{600} (0.7 m^2/g) and Fe_3O_4/C-SO_3H_{700} (0.6 m^2/g) (Table 1). This might be caused by the higher calcination temperature causing Fe_3O_4 to be embedded in the pores.

The XRD peaks of the three catalysts were all identified as the crystalline phase of Fe_3O_4 (Fig. 2), which indicated that Fe_3O_4 remained stable after calcination and sulfonation during the preparation of catalysts. In FTIR analysis, the absorption peak at 598 cm^{-1} was the Fe-O bond vibration in Fe_3O_4 (Fig. 3) (Guo *et al.,* 2013). The absorption peaks at 1600-1800 cm^{-1} were C=C, C=O and COO^- stretching vibrations and 3463 cm^{-1} was -OH stretching vibration (Alvaro *et al.,* 2005). The absorption peaks at 1061 cm^{-1} (-SO_3^- stretching) and the 1223 cm^{-1} (O=S=O stretching in -SO_3H) were important signs of the presence of -SO_3H functional groups (Fukuhara *et al.,* 2011). All peak strengths of Fe_3O_4/C-SO_3H_{500} were weak. The difference between Fe_3O_4/C-SO_3H_{600} and Fe_3O_4/C-SO_3H_{700} was that catalyst Fe_3O_4/C-SO_3H_{600} appeared-SO_3^- stretching and O=S=O stretching in -SO_3H at bands 1061 cm^{-1} and 1223 cm^{-1}, respectively. This showed the presence of -SO_3H functional group in Fe_3O_4/C-SO_3H_{600}. NH_3-TPD characterization also indicated that the acid sites of Fe_3O_4/C-SO_3H_{600} (0.7 mmol/g) were higher than that of Fe_3O_4/C-SO_3H_{500} (0.1 mmol/g) and

Fe_3O_4/C-SO_3H_{700} (0.5 mmol/g) (Table 1).

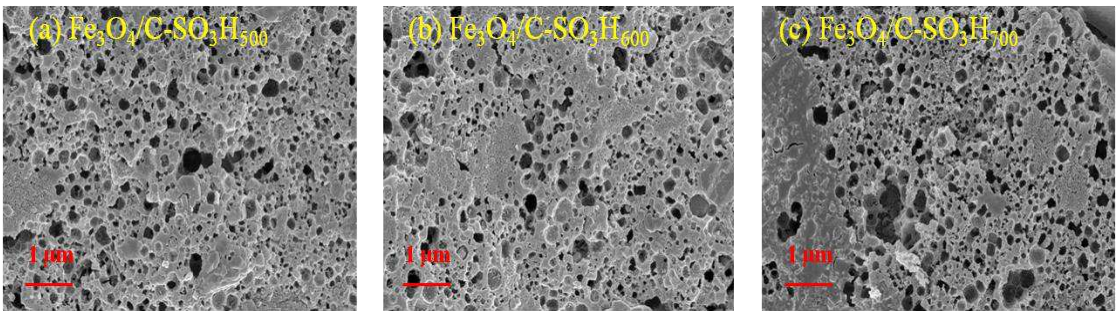

Figure 1. SEM images of catalysts.

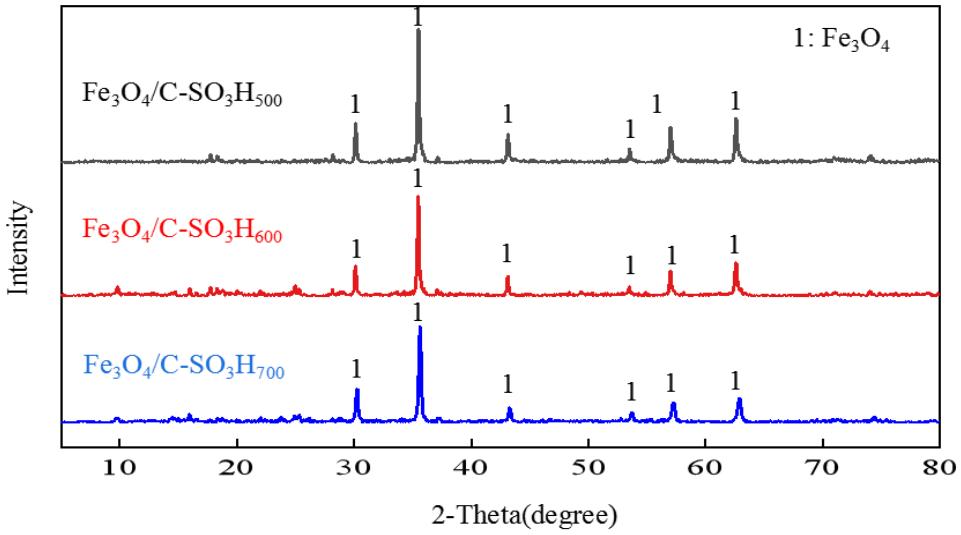

Figure 2. XRD patterns of catalysts.

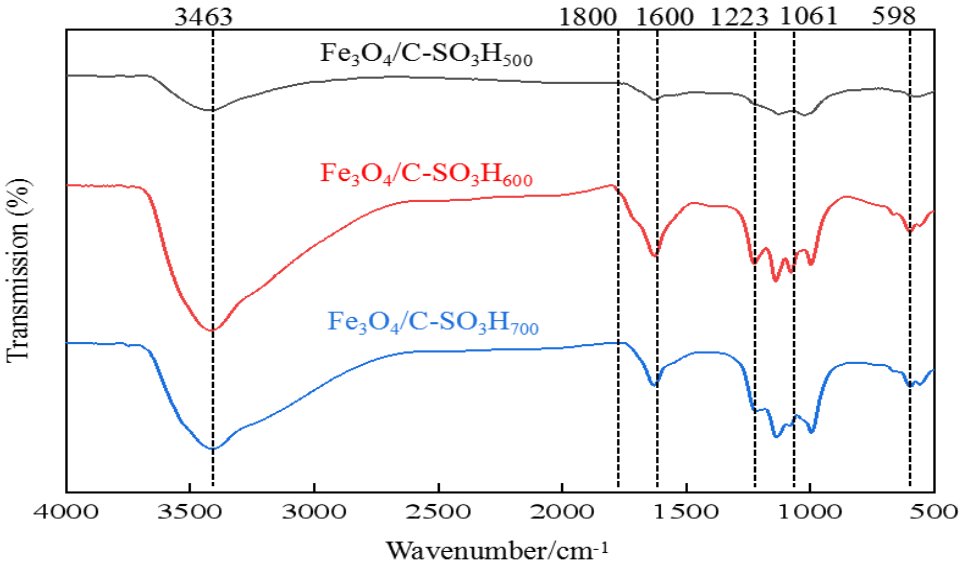

Figure 3. FTIR analysis of catalysts.

Table 1. The total acid sites and textural properties of the catalysts

Catalysts	Acid sites (mmol/g)	BET surface area (m^2/g)	Pore volume (cm^3/g)
Fe_3O_4/C-SO_3H_{500}	0.1	1.8	0.006
Fe_3O_4/C-SO_3H_{600}	0.7	0.7	0.006
Fe_3O_4/C-SO_3H_{700}	0.5	0.6	0.002

TG and kinetic analysis

The TG analysis of pure cellulose and cellulose mixed with the solid acid catalyst is shown in Fig. 4 and Table 2. The main weight loss area of cellulose was 300-400 °C, and after mixing with the solid acid, the main weight loss area shifted to 200-400 °C. Considering the heating rate was 40 °C/min, the initial weight loss temperature of cellulose was 335 °C, which was higher than that of cellulose mixed with catalysts (199-263 °C). D_{max} was the maximum weight loss rate in the decomposition reaction process, which indicated the degree of the decomposition reaction. The greater the D_{max} was, the more intense the decomposition reaction revealed. The D_{max} of cellulose (2.0-2.8%/°C) was also higher than that of cellulose mixed with the solid acid catalysts (0.2-0.7%/°C). The reason was that the thermal stability of cellulose was high, the thermal decomposition was carried out at a higher temperature and the reaction was concentrated, while the thermal stability of cellulose mixed with the catalyst was reduced, resulting in the dispersed decomposition reaction, and the wide main weight loss area.

The DAEM is currently the most accurate thermal analysis kinetic model, which can accurately simulate the experimental curve, as shown in Fig. 5. The kinetic parameters calculated according to DAEM are shown in Table 3. *E* referred to the global activation energy, that was, the energy that needed to be absorbed when the sample was decomposed. The larger the *E*, the more energy needed to be absorbed

during the decomposition, and the more difficult it was to decompose. σ refers to the deviation of activation energy, which indicates the concentration of decomposition reaction. Consider the heating rate was 40 °C/min, compared with the cellulose mixed with the catalyst (168.1-175.5 kJ/mol), the cellulose had the highest activation energy (187.4 kJ/mol). After mixed with the catalyst, activation energy for cellulose decomposition was reduced, thereby reducing the initial decomposition temperature. In addition, the σ of cellulose (0.1 kJ/mol) was the smallest and the reaction was the most concentrated, while the cellulose mixed with catalyst had larger σ, and the reaction was dispersed. It could be seen that the thermal stability of cellulose could be destroyed after adding the catalyst, and the cellulose could be decomposed at a lower temperature.

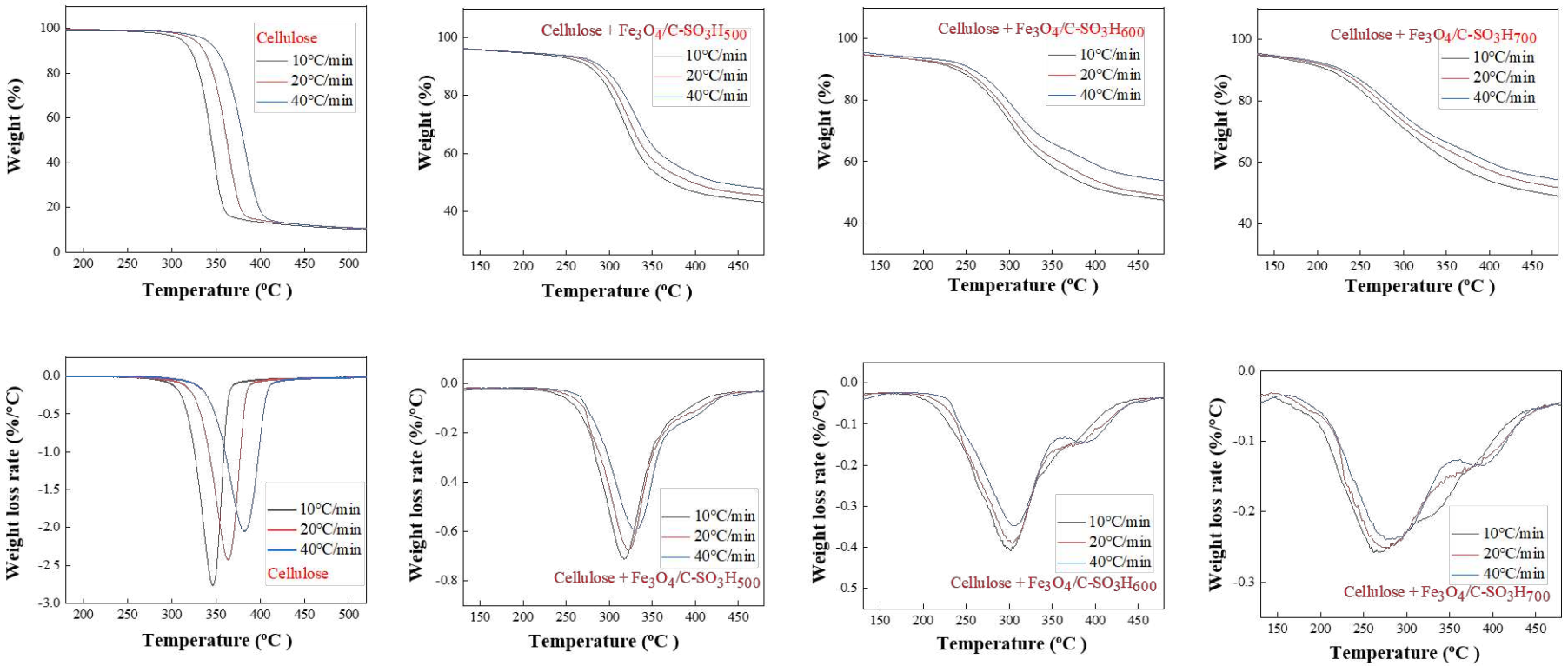

Figure 4. TG and DTG curves of cellulose and cellulose mixed with catalyst.

Table 2. Thermogravimetric parameters at different heating rates

Samples	Heating rates (°C/min)	T_i (°C)	T_t (°C)	T_{max} (°C)	D_{max} (%/°C)
Cellulose	10	308	368	346	-2.8
	20	322	383	363	-2.4
	40	335	403	381	-2.0
Cellulose + Fe_3O_4/C-SO_3H_{500}	10	250	413	317	-0.7
	20	257	419	323	-0.7
	40	263	425	329	-0.6
Cellulose + Fe_3O_4/C-SO_3H_{600}	10	218	424	300	-0.4
	20	225	430	304	-0.4
	40	227	434	307	-0.3
Cellulose + Fe_3O_4/C-SO_3H_{700}	10	193	437	267	-0.3
	20	197	440	275	-0.3
	40	199	441	286	-0.2

T_i is the temperature of pyrolysis at which the main weightless zone begins, 5%.
T_t is the temperature of pyrolysis at which the main weightless zone finishes, 95%.
T_{max} is the temperature corresponding to the highest point of the DTG peak.
D_{max} is the weight loss rate corresponding to the highest point of the DTG peak.

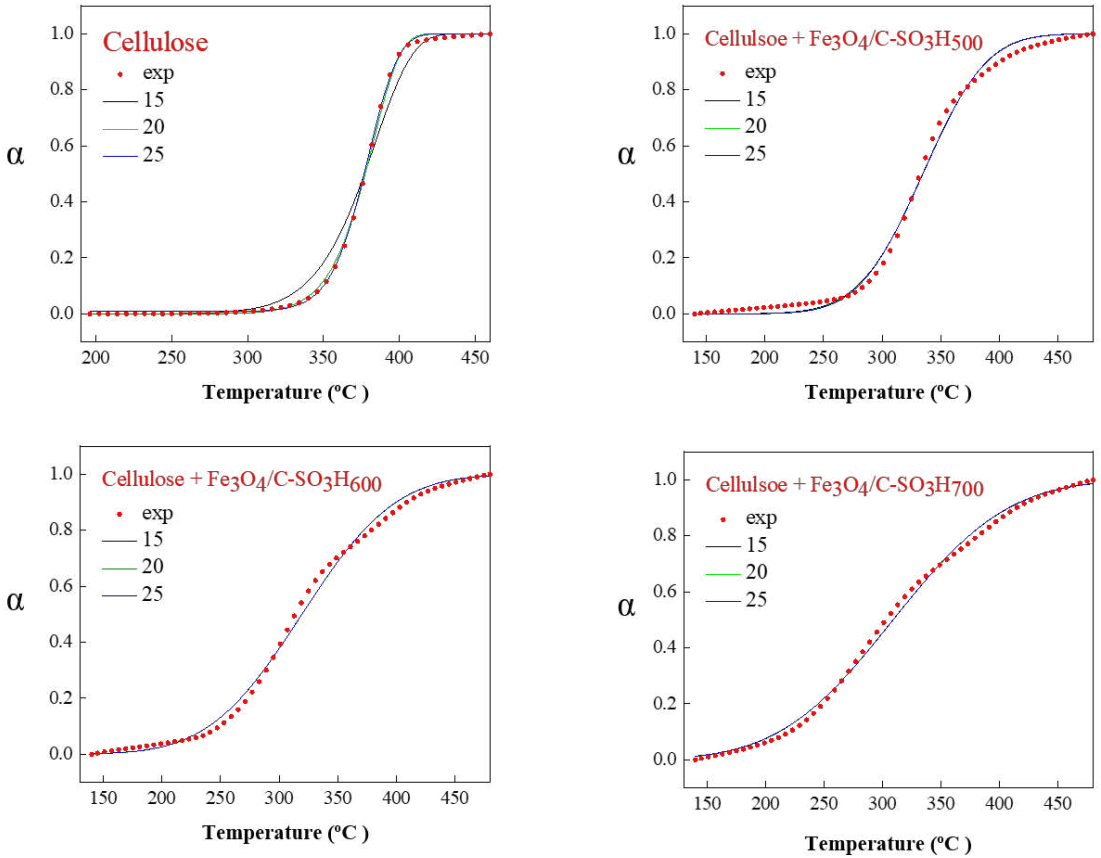

227

228 Figure 5. The experimental curve and curve fitted by DAEM model.

229

Table 3. Kinetic parameters on the basis of the distributed activation energy model

Samples	lgA (s^{-1})	E (kJ/mol)	σ (kJ/mol)	R^2	Compensation effect
Cellulose	15	187.4	0.1	0.9992	E=5.1915lnA+8.0246 R^2=1
	20	246.9	3.6	0.9996	
	25	307.0	6.1	0.9994	
Cellulose + Fe_3O_4/C-SO_3H_{500}	15	175.5	11.3	0.9963	E=4.8464lnA+8.0474 R^2=1
	20	231.1	15.5	0.9964	
	25	287.1	19.6	0.9964	
Cellulose + Fe_3O_4/C-SO_3H_{600}	15	171.1	17.6	0.9967	E=4.7249lnA+7.8654 R^2=1
	20	225.3	23.5	0.9967	
	25	279.9	29.4	0.9967	
Cellulose + Fe_3O_4/C-SO_3H_{700}	15	168.1	22.0	0.9975	E=4.6415lnA+7.6873 R^2=1
	20	221.3	29.2	0.9975	
	25	275.0	36.3	0.9974	

Effect of different catalysts on the yield of LGO

The yield of LGO prepared by fast pyrolysis of pure cellulose and fast pyrolysis of cellulose catalyzed by different catalysts was shown in Fig. 6. The yield and relative content of LG were also analyzed as it was the main product in non-catalytic pyrolysis of cellulose. During the non-catalytic pyrolysis of pure cellulose, the yield and relative content of LG were as high as 38.6 wt% and 84.3%, respectively, while the yield (0.3 wt%) and relative content (0.9%) of LGO in the pyrolysis products were very low. In catalytic pyrolysis of cellulose, both the yield and relative content of LG decreased significantly. It could be seen from the different cellulose pyrolysis results that there was a significant negative correlation between the production of LG and LGO, which should be further analyzed. The higher the yield and relative content of LGO was, the more obvious the decrease in the yield and relative content of LG obtained. Fe_3O_4 and acidic sites -SO_3H enhanced the dehydration behavior in the cellulose pyrolysis process, which was the main reason for the improvement in LGO yield. The yield of LGO (20.0 wt%) in the pyrolysis product was obtained from cellulose catalyzed by Fe_3O_4/C-SO_3H_{600}, which was higher than that from cellulose catalyzed by Fe_3O_4/C-SO_3H_{500} (4.2 wt%) and Fe_3O_4/C-SO_3H_{700} (13.5 wt%). The functional groups and acidic sites in the catalyst were the keys to promoting the formation of LGO. Fe_3O_4/C-SO_3H_{500} had fewer functional groups and acidic sites, causing the poor catalytic effect. Fe_3O_4/C-SO_3H_{600} exhibited more -SO_3H functional groups than Fe_3O_4/C-SO_3H_{700}. Furthermore, Fe_3O_4/C-SO_3H_{600} had the highest acidic site, which might also an important factor to promote the formation of LGO. Fe_3O_4/C-SO_3H_{600} had the best catalytic effect, and its reaction condition was further optimized.

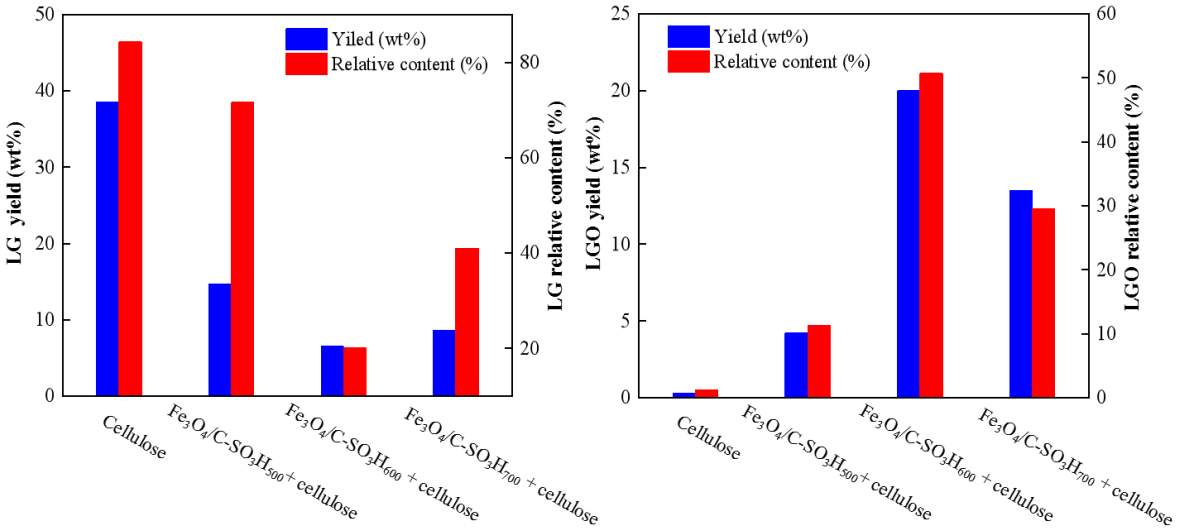

Figure 6. The effect of three catalysts to pyrolyze cellulose on the yield and relative content of LG and LGO.

Effects of the catalytic pyrolysis temperature on the yield of LGO

The distribution of pyrolysis products could vary with temperature as the dominant reaction pathways shifted in rate and overall extent (Maduskar *et al.,* 2018). Fig. 7 shows the yield and relative content of LG and LGO at different temperatures during non-catalytic and catalytic pyrolysis. As the temperature increased, the cellulose was fully depolymerized and accompanied by a series of competitive reactions. The yield of LG increased from 38.6 wt% to 60.1 wt% as the temperature increased from 300 °C to 500 °C, while the yield of LGO (0.2 wt%-0.3 wt%) was very low. As depicted in Fig. 8a, LG and 1,6-anhydro-.beta.-D-glucofuranose (AGF) were the main products obtained by non-catalytic fast pyrolysis of cellulose at 300 °C, with relative content of 79% and 8%, respectively. As the temperature rose from 300 °C to 500 °C under non-catalytic pyrolysis conditions, the main products of cellulose pyrolysis were still LG and AGF, but hydroxyacetaldehyde (HAA), furfural (FF), 5-hydromethyl-furfural (5-HMF) and other compounds were also produced. Although the increase in temperature was accompanied by a series of competitive reactions that led to a decrease in the relative content of LG, the increase in

temperature also made the cellulose fully depolymerized resulting in the increasing yield of LG.

The catalytic pyrolysis of cellulose with Fe_3O_4/C-SO_3H_{600} could promote the formation of LGO and inhibit the formation of LG and AGF. The increase in the yield of LGO might be caused by the catalytic dehydration of LG. The promotion on LGO production was more obvious at 300 °C. According to Fig. 8b, it could be seen that the primary pyrolysis product of catalytic fast pyrolysis of cellulose at 300 °C was transformed from LG to LGO, accompanied by a certain amount of 1,4:3,6-dianhydro-α-d-glucopyranose (DGP). During catalytic pyrolysis, the LGO yield tended to increase at 250-300 °C and then decrease at 300-500 °C. The highest yield of LGO (20.0 wt%) was obtained at 300 °C and the lowest LGO yield was got at 500 °C (4.9 wt%). The relative content of LGO also increased at 250-300 °C, and then decreased at 300-500 °C. The low yield and relative content of LGO at 250 °C could be attributed to the incomplete decomposition of cellulose and the difficulty in providing enough heat to enable the Fe_3O_4/C-SO_3H_{600} to catalyze the dehydration of cellulose. Catalytic fast pyrolysis could effectively reduce the competitive reaction in the cellulose pyrolysis process at 500 °C, and make the product distribution concentrate on the anhydrosugars LG, LGO, and DGP (Fig. 8d). The formation of LGO was mainly through glycosidic bond cleavage reactions in which cellulose was depolymerized and then exposed on dehydration reactions of the pyran ring. The dehydration process was the main reactions that affected the formation of LGO, mainly occurred at low temperatures, and the cleavage of glycosidic bonds mainly occurred in the medium temperature. As the pyrolysis temperature increased, the rate of cellulose glycosidic bond cleavage reaction was accelerated. When it was faster than the dehydration rate, only a small part of the glycosidic bond cleavage product

could be dehydrated, which limited the production of LGO, resulting in the reduction of LGO production at 300-500 °C in catalytic pyrolysis. These results also demonstrated that Fe_3O_4/C-SO_3H_{600} could not only promote the formation of LGO, but also reduced the pyrolysis temperature of cellulose.

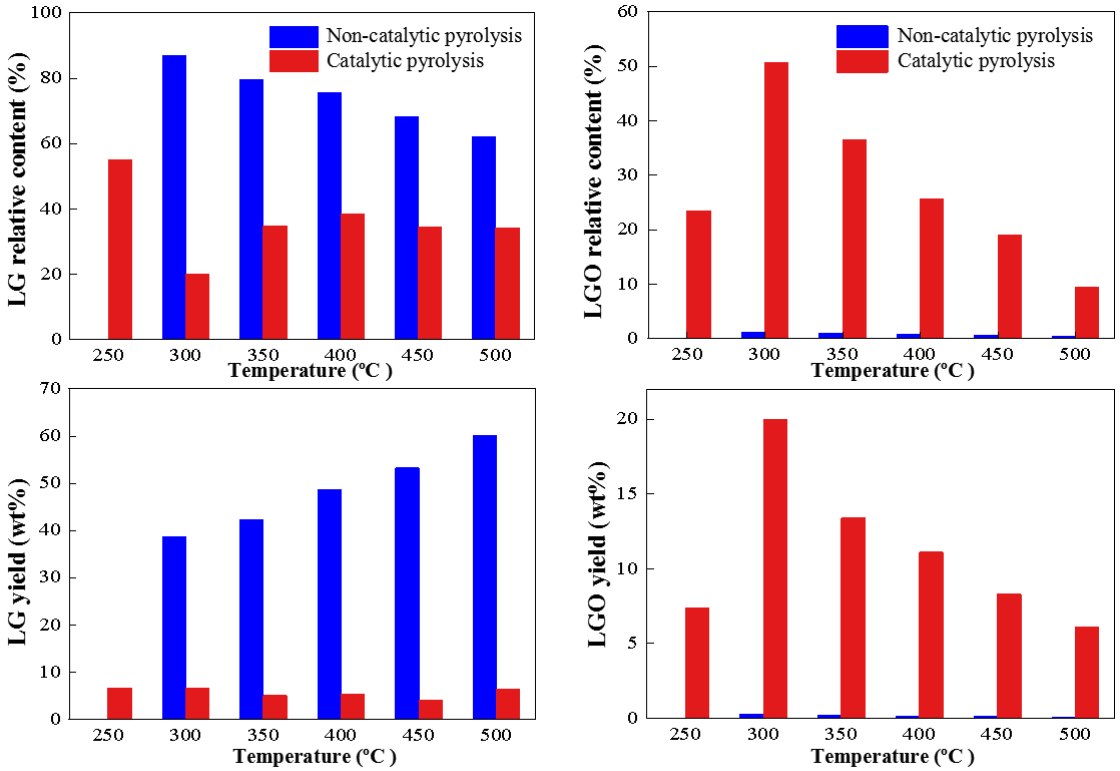

Figure 7. Effect of the temperature on the relative content and yield of LG and LGO.

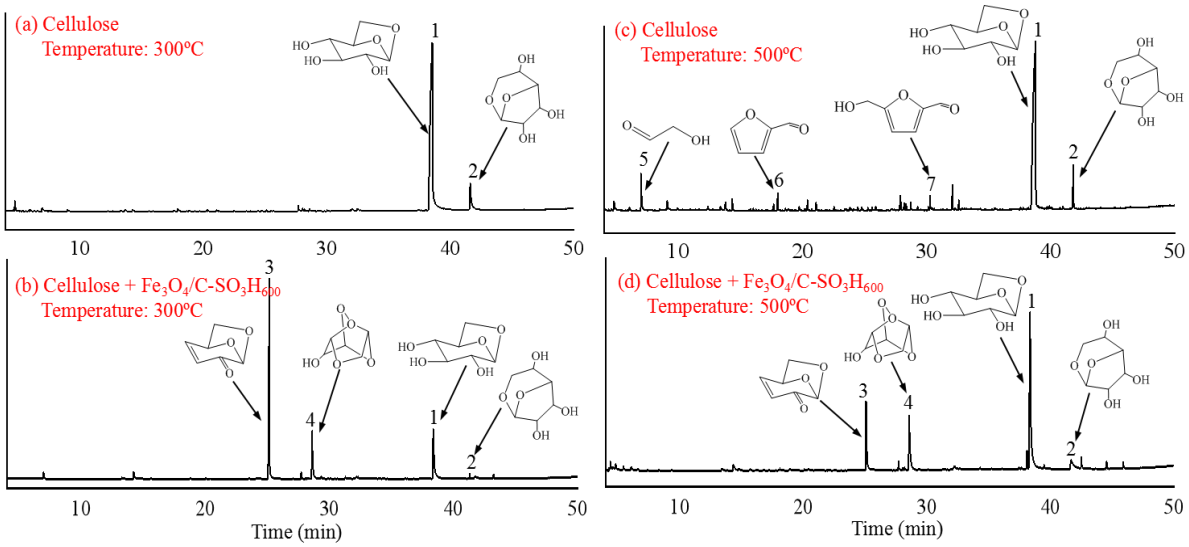

Figure 8. Typical ion chromatograms of cellulose pyrolysis: (a) cellulose in noncatalytic pyrolysis at 300 °C, (b) cellulose in catalytic pyrolysis at 300 °C, (c) cellulose in noncatalytic pyrolysis at 500 °C, (d) cellulose in catalytic pyrolysis at 500 °C, (1) LG, (2) AGF, (3) LGO, (4) DGP, (5) HAA, (6) FF, (7) 5-HMF.

Effect of the Fe_3O_4/C-SO_3H_{600} to cellulose ratio

The ratio of Fe_3O_4/C-SO_3H_{600} to cellulose is also an important factor affecting the distribution of pyrolysis products. With the increase in the amount of catalyst, the yield and relative content of LGO showed a trend of initially increasing followed by a decrease, while the yield and relative content of LG continued to decrease as the amount of catalyst increased (Fig. 9). This showed that when the amount of catalyst was increased, the conversion of LG to LGO was promoted. The best ratio of Fe_3O_4/C-SO_3H_{600} to cellulose was 1:1, in which the yield and relative content of LGO were 20.0 wt% and 50.7%, respectively. When the ratio of Fe_3O_4/C-SO_3H_{600} to cellulose rose from 1:3 to 1:1, the acidic sites of the catalyst gradually increased, and the cellulose was able to completely contact the catalyst, so the yield of LGO continued to rise. When the ratio of Fe_3O_4/C-SO_3H_{600} to cellulose increased from 1:1 to 3:1, the relative content of LGO changed a little, but the yield of LGO decreased to 12.6 wt%, which indicated that the excess catalyst exhibited a negative effect on the yield of LGO. The conclusion could be depicted as: first, an excessive amount of

catalyst would increase the heat transfer resistance of the sample, making it difficult for heat energy to accurately act on the catalytic reaction, thereby weakening the catalytic effect (Mullen and Boateng, 2010). Second, dehydration and charring reactions of cellulose were boosted by excessive catalyst, resulting in the reduction of organic volatile products (Branca *et al.,* 2011). In addition, excess catalyst might also catalyze further reactions of LGO, leading to reduction in LGO yield (Bai *et al.,* 2019).

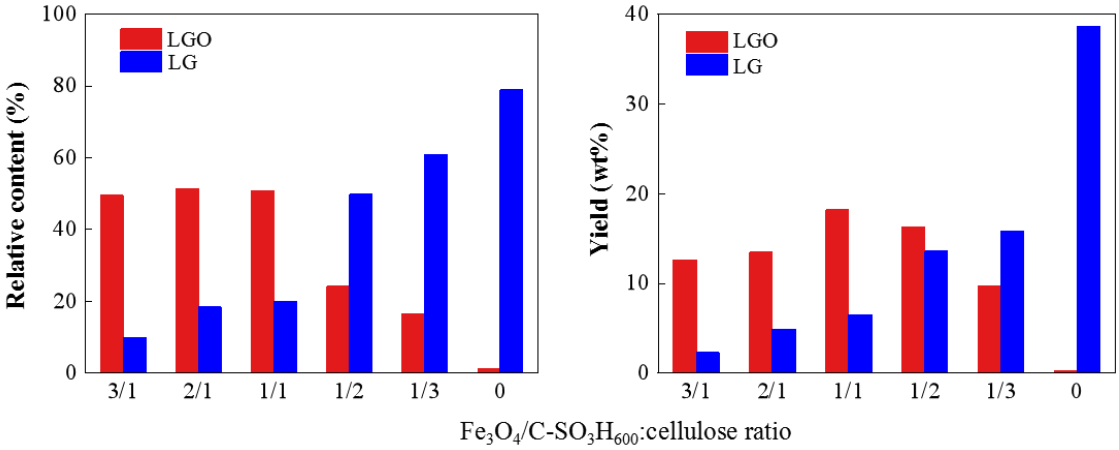

Figure 9. Effect of Fe_3O_4/C-SO_3H_{600}-to-cellulose ratio on the relative content and yield of LG and LGO at 300 °C.

Recycling of the catalyst

In order to evaluate the stability of the catalyst, the reuse of Fe_3O_4/C-SO_3H_{600} for LGO production was repeatedly conducted under the optimum conditions of 300 °C and the ratio of cellulose to catalyst of 1:1. As shown in Fig. 10, the yields of LGO in the three cycle experiments were 14.1 wt%, 11.6 wt%, and 8.3 wt%, respectively. This showed that the catalyst could still effectively increase the yield of LGO in the cellulose pyrolysis product after undergoing the cycle experiment, but the acid sites in the catalyst might fall off during multiple cycles, so the catalyst effect of catalyst was significantly reduced. To improve the circulated feasibility the catalyst, the three-cycled catalyst was mixed with H_2SO_4 and sulfonated at 150 °C for 20 h for regeneration. The results of fast pyrolysis showed that the catalytic activity of the

regenerated catalyst was completely restored, and the yield of LGO reached 20.6 wt%. Compared with catalysts such as liquid acids and ionic liquids, Fe_3O_4/C-SO_3H_{600} could not only efficiently catalyze the production of LGO from cellulose, but also could be recycled and reused, which was more economical and practical.

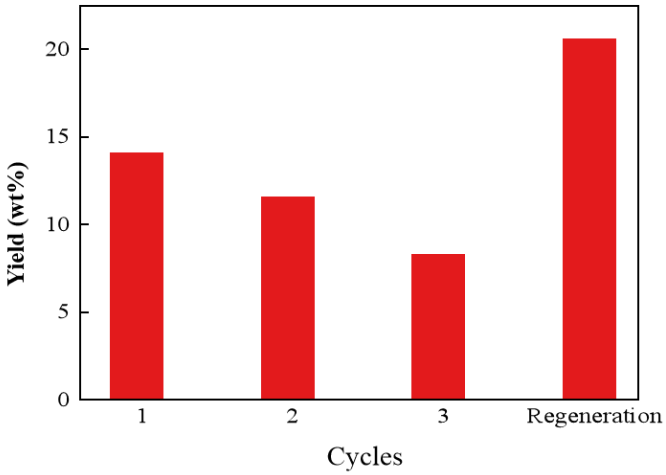

Figure 10. Effect of catalyst cycle on LGO yield at 300 °C.

The mechanism of fast pyrolysis of cellulose to LGO

According to currently proposed views, there were two main ways to produce LGO. First, cellulose was pyrolyzed and depolymerized to produce LG, and LG was further dehydrated to produce LGO. Second, cellulose was first dehydrated during pyrolysis, and then the glycoside bonds at both ends were broken to form LGO (Zhang *et al.,* 2017; Lu *et al.,* 2011). The latter process did not produce LG. In this experiment, since the increase in LGO yield was consistent with the decrease in LG yield, it was speculated that Fe_3O_4/C-SO_3H_{600} could promote further dehydration of LG to produce LGO. To verify it, pure LG was mixed with Fe_3O_4/C-SO_3H_{600} for fast pyrolysis at 300 °C. The typical ion chromatogram was shown in Fig. 11. The results showed that the presence of Fe_3O_4/C-SO_3H_{600} could indeed catalyze the dehydration of LG to produce LGO and DGP. It is noticeable that although LGO and DGP were both products of LG's further dehydration, the increase in the yield of LGO was

significantly more than that of DGP. This showed that the catalytic effect of Fe_3O_4/C-SO_3H_{600} was also selective. After observing the chemical structure of the three anhydrosugars, it could be found that LG and LGO had similar bicyclic structures (1,5- and 1,6-acetal rings). The conversion of LG to LGO only required dehydration to form C_2 carbonyl and C_3=C_4 bonds. The conversion from LG to DGP initially requires intramolecular transglycosylation to form 1,4-anhydride, and then etherification to form 3,6-anhydride (Shafizadeh *et al.,* 1978). The latter was more complicated. This explained that Fe_3O_4/C-SO_3H_{600} selectively catalyzed the dehydration of LG to LGO instead of DGP during the pyrolysis of cellulose. A possible pathway for the production of LGO by catalytic pyrolysis of cellulose was presented in Fig. 12. First, cellulose broke the glycosidic bonds on both sides by thermal pyrolysis to produce LG. Then LG was further dehydrated under acid catalysis to generate LGO. In this procedure, S1 with the carbon-carbon double bonds was produced through 3-OH obtained H (Lu *et al.,* 2014b). Acid catalysis caused this reaction and promoted its dehydration. Then a keto-enol tautomerism reaction occurred to form a carbon-oxygen double bonds (S2). After these conversions were completed, acid catalysis caused S2 to lose another molecule of H_2O to produce LGO.

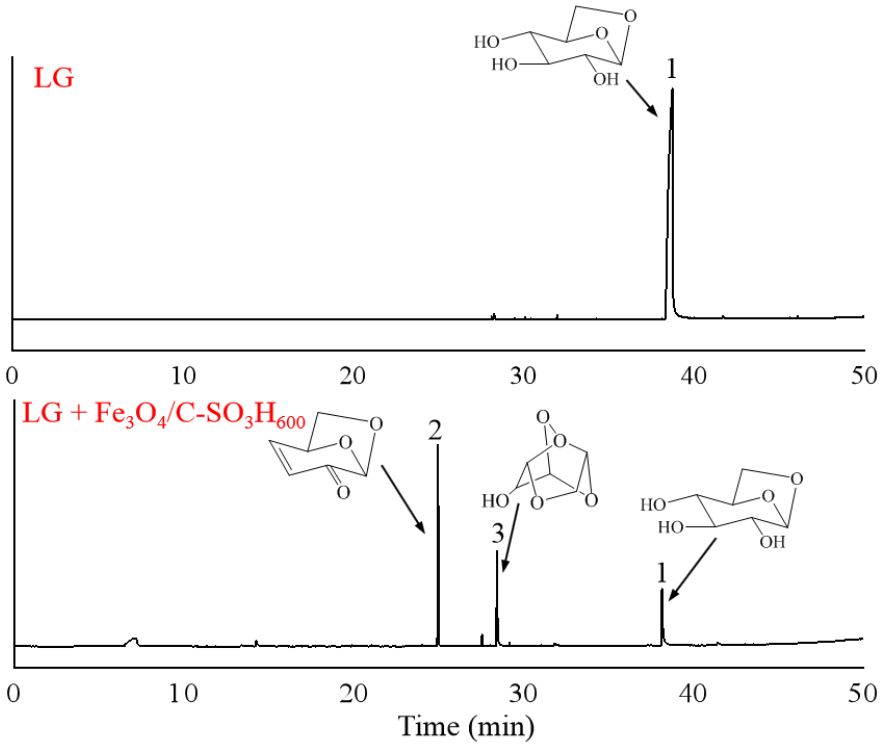

Figure 11. Typical ion chromatograms of LG in noncatalytic and catalytic pyrolysis: (1) LG, (2) LGO, (3) DGP.

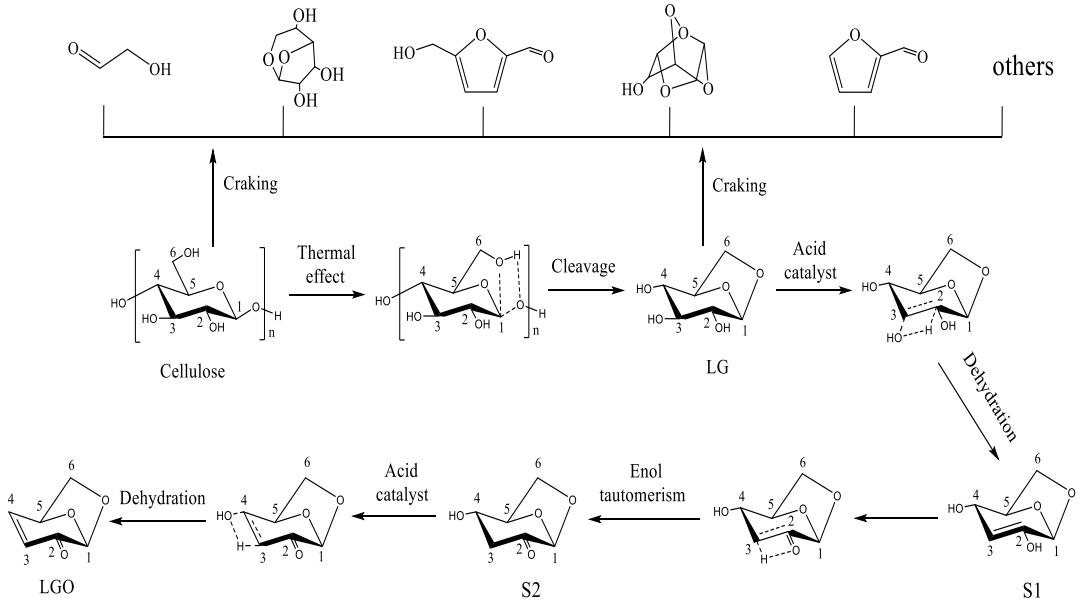

Figure 12. Possible reaction mechanism of catalytic fast pyrolysis of cellulose for LG and LGO production.

Conclusions

Magnetic solid acid Fe_3O_4/C-SO_3H_{600} was prepared to catalyze fast pyrolysis of cellulose for the selective production of LGO. The yield of LGO was increased from 0.3 wt% to 20.0 wt% at a pyrolysis temperature of 300 °C. The catalytic pyrolysis of cellulose could not only reduce the reaction-required temperature and promote the LGO production, but also could be reused for recycling in an economical and practical approach. In addition, this study explored the mechanism of cellulosic pyrolysis to produce LGO, indicating that LGO could be produced via further dehydration of LG.

Declarations

Not applicable.

Funding

This work was funded by the National Natural Science Foundation of China (No. 51606204), the Science and Technology Planning Project of Guangzhou city and Guangdong province (No. 2017A020216007, 201707010236).

Conflict of Interest

The authors declare that they have no conflict of interest.

References

Alvaro M, Corma A, Das D, Fornes V, Garcia, H (2005) "Nafion"-functionalized mesoporous MCM-41 silica shows high activity and selectivity for carboxylic acid esterification and Friedel-Crafts acylation reactions. J Catal 231(1):48-55. https://doi.org/10.1016/j.jcat.2005.01.007.

Bai XW, Li J, Jia CX, Shao JA, Yang Q, Chen YQ, Yang HP, Wang XH, Chen HP (2019) Preparation of furfural by catalytic pyrolysis of cellulose based on nano Na/Fe-solid acid. Fuel 258:116089. https://doi.org/10.1016/j.fuel.2019.116089.

Branca C, Galgano A, Blasi C, Esposito M, Blasi CD (2011) H_2SO_4-catalyzed pyrolysis of corncobs. Energy Fuels 25(1):359-369. https://doi.org/10.1021/ ef101317f.

Cao F, Schwartz TJ, McClelland DJ., Krishna SH, Dumesic JA, Huber GW (2015) Dehydration of cellulose to levoglucosenone using polar aprotic solvents. Energy Environ Sci 8(6):1808-1815. https://doi.org/10.1039/c5ee00353a.

Dobele G, Rossinskaja G, Telysheva G, Meier D, Faix O (1999) Cellulose dehydration and depolymerization reactions during pyrolysis in the presence of phosphoric acid. J Anal Appl

Pyrolysis 49(1-2):307-317. https://doi.org/10.1016/ S0165-2370(98)00126-0.
Doroshenko A, Pylypenko I, Heaton K, Cowling S, Clark J, Budarin V (2019) Selective microwave-assisted pyrolysis of cellulose towards levoglucosenone with clay catalysts. ChemSusChem 12(24):5224-5227. https://doi.org/10.1002/cssc. 201903026.
Fukuhara K, Nakajima K, Kitano M, Kato H, Hayashi S, Hara M (2011) Structure and catalysis of cellulose-derived amorphous carbon bearing SO_3H groups. ChemSusChem 4(6):778-784. https://doi.org/10.1002/cssc.201000431.
Guo HX, Lian YF, Yan LL, Qi XH, Smith RL (2013) Cellulose-derived superparamagnetic carbonaceous solid acid catalyst for cellulose hydrolysis in ionic liquid or aqueous reaction system. Green Chem 15(8):2167-2174. https://doi. org/10.1039/c3gc40433a.
Halpern Y, Riffer R, Broido A (1973) Levoglucosenone (1,6-anhydro-3,4-dideoxy-.DELTA.3-.beta.-D-pyranosen-2-one). Major product of the acid-catalyzed pyrolysis of cellulose and related carbohydrates. J Org Chem 38(2):204-209. https://doi.org/10.1021/jo00942a005.
Jiang LQ, Lin QL, Lin Y, Xu FX, Zhang X, Zhao ZL, Li HB (2020a) Impact of ball-milling and ionic liquid pretreatments on pyrolysis kinetics and behaviors of crystalline cellulose. Bioresour Technol 305:123044. https://doi.org/10.1016/j. biortech.2020.123044.
Jiang LQ, Wu YX, Zhao ZL, Li HB, Zhao K, Zhang F (2020b) Selectively biorefining levoglucosan from NaOH pretreated corncobs via fast pyrolysis. Cellulose 26:7877-7887. https://doi.org/10. 1007/s10570-019-02625-4.
Kudo S, Goto N, Sperry J, Narinaga K, Hayashi J (2017) Production of levoglucosenone and dihydrolevoglucosenone by catalytic reforming of volatiles from cellulose pyrolysis using supported ionic liquid phase. ACS Sustain Chem Eng 5(1):1132-1140. https://doi.org/10.1021/ acssuschemeng.6b02463.
Liu X, Carr P, Gardiner MG, Banwell MG, Elbanna AH, Zeinab G, Capon RJ (2020) Levoglucosenone and its pseudoenantiomer iso-levoglucosenone as scaffolds for drug discovery and development. ACS Omega 5(23):13926-13939. https://doi. org/10.1021/acsomega.0c01331.
Lu Q, Yang XC, Dong CQ, Zhang ZF, Zhang, XM, Zhu XF (2011) Influence of pyrolysis temperature and time on the cellulose fast pyrolysis products: Analytical Py-GC/MS study. J Anal Appl Pyrolysis 92(2):430-438. https://doi.org/10.1016/j. jaap.2011.08.006.
Lu Q, Ye XN, Zhang ZB, Dong CQ, Zhang Y (2014a) Catalytic fast pyrolysis of cellulose and biomass to produce levoglucosenone using magnetic SO_4^{2-}/TiO_2-Fe_3O_4. Bioresour Technol 171:10-15. https://doi.org/10.1016/j.biortech.2014.08. 075.
Lu Q, Zhang Y, Dong CQ, Yang YP, Yu HZ (2014b) The mechanism for the formation of levoglucosenone during pyrolysis of beta-D-glucopyranose and cellobiose: A density functional theory study. J Anal Appl Pyrolysis 110:34-43. https://doi.org/10.1016/j.jaap.2014.08.002.
Maduskar S, Maliekkal V, Neurock M, Dauenhauer PJ (2018) On the yield of levoglucosan from cellulose pyrolysis. ACS Sustain Chem Eng 6(5):7017-7025. https://doi.org/10.1021/acssus chemeng.8b00853.
Meng X, Zhang HY, Liu C, Xiao R (2016) Comparison of acids and sulfates for producing levoglucosan and levoglucosenone by selective catalytic fast pyrolysis of cellulose using Py-GC/MS. Energy Fuels 30(10):8369-8376. https://doi.org/10. 1021/acs.energyfuels.6b01436.
Mullen CA, Boateng AA (2010) Catalytic pyrolysis-GC/MS of lignin from several sources. Fuel Process Technol 91(11):1446-1458. https://doi.org/10.1016/j.fuproc. 2010.05.022.
Shafizadeh F, Furneaux RH, Stevenson TT, Cochran TG (1978) Acid-catalyzed pyrolytic synthesis and decomposition of 1,4-3,6-dianhydro-alpha-d-glucopyranose. Carbohydr Res 61(1):519-528. https://doi.org/10.1016/S0008-6215(00)84510-3.
Sharifzadeh M, Sadeqzadeh M, Guo M, Borhani TN, Konda NVSNM, Garcia MC, Wang L, Hallett J, Shah N (2019) The multi-scale challenges of biomass fast pyrolysis and bio-oil upgrading: Review of the state of art and future research directions. Prog Energy Combust Sci 71:1-80. https://doi.org/10.1016/j.pecs.2018. 10.006.
Tshikesho RS, Kumar A, Huhnke RL, Apblett A (2019) Catalytic co-pyrolysis of red cedar with methane to produce upgraded bio-oil. Bioresour Technol 285:121299. https://doi.org/10.1016/j. biortech.2019.03.138.
Usino DO, Supriyanto, Ylitervo P, Pettersson A, Richards T (2020) Influence of temperature and time on initial pyrolysis of cellulose and xylan. J Anal Appl Pyrolysis 147:104782. https://doi.org/10. 1016/j.jaap.2020.104782.
Wang Z, Lu Q, Zhu XF, Zhang Y (2011) Catalytic fast pyrolysis of cellulose to prepare levoglucosenone using sulfated zirconia. ChemSusChem 4(1):79-84. https://doi.org/10.1002/cssc. 201000210.
Ye XN, Lu Q, Wang X, Guo HQ, Cui MS, Dong CQ, Yang YP (2017) Catalytic fast pyrolysis of

cellulose and biomass to selectively produce levoglucosenone using activated carbon catalyst. ACS Sustain Chem Eng 5(11):10815-10825. https://doi. org/10.1021/acssuschemeng.7b02762.

Zhang F, Xu LJ, Xu FX, Jiang LQ (2021) Different acids pretreatments at room temperature boost selective saccharification of lignocellulose via fast pyrolysis. Cellulose 28:81-90. https://doi.org/10.1007/s10570-020-03544-5.

Zhang HY, Meng X, Liu C, Wang Y, Xiao R (2017) Selective low-temperature pyrolysis of microcrystalline cellulose to produce levoglucosan and levoglucosenone in a fixed bed reactor. Fuel Process. Technol 167:484-490. https://doi.org/10.1016/j.fuproc.2017.08.007.

Zhang JK, Xu YJ, Wang WQ, Griffin J, Roozeboom K, Wang DH (2020) Bioconversion of industrial hemp biomass for bioethanol production: A review. Fuel 281:118725. https://doi.org/10.1016/j.fuel.2020.118725.

Zhang Y, Lei H, Yang Z, Qian K, Villota E (2018) Renewable high-purity mono-phenol production from catalytic microwave-induced pyrolysis of cellulose over biomass-derived activated carbon catalyst. ACS Sustain Chem Eng 6(4):5349-5357. https://doi.org/10.1021/acssuschemeng.8b00129.

Figures

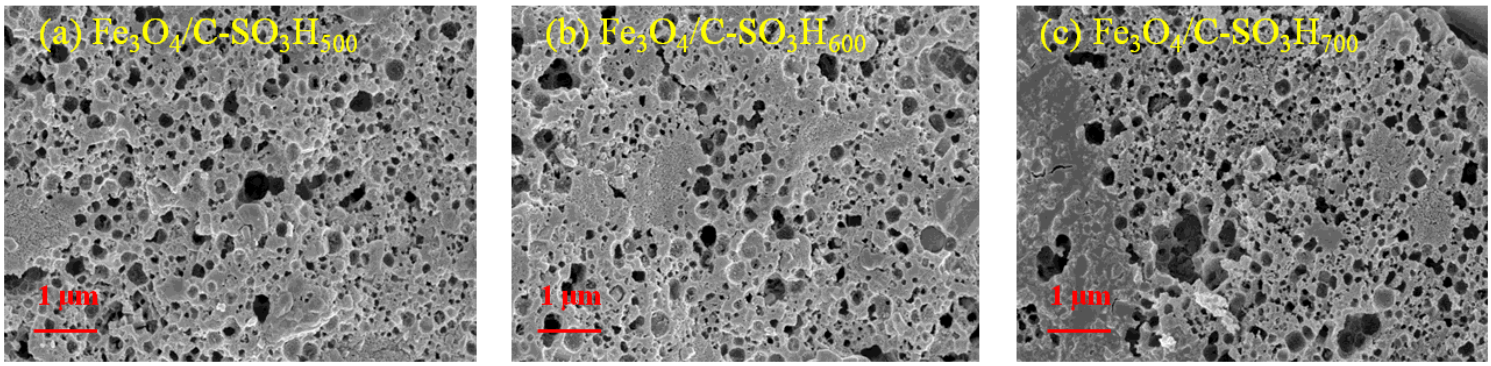

Figure 1

SEM images of catalysts.

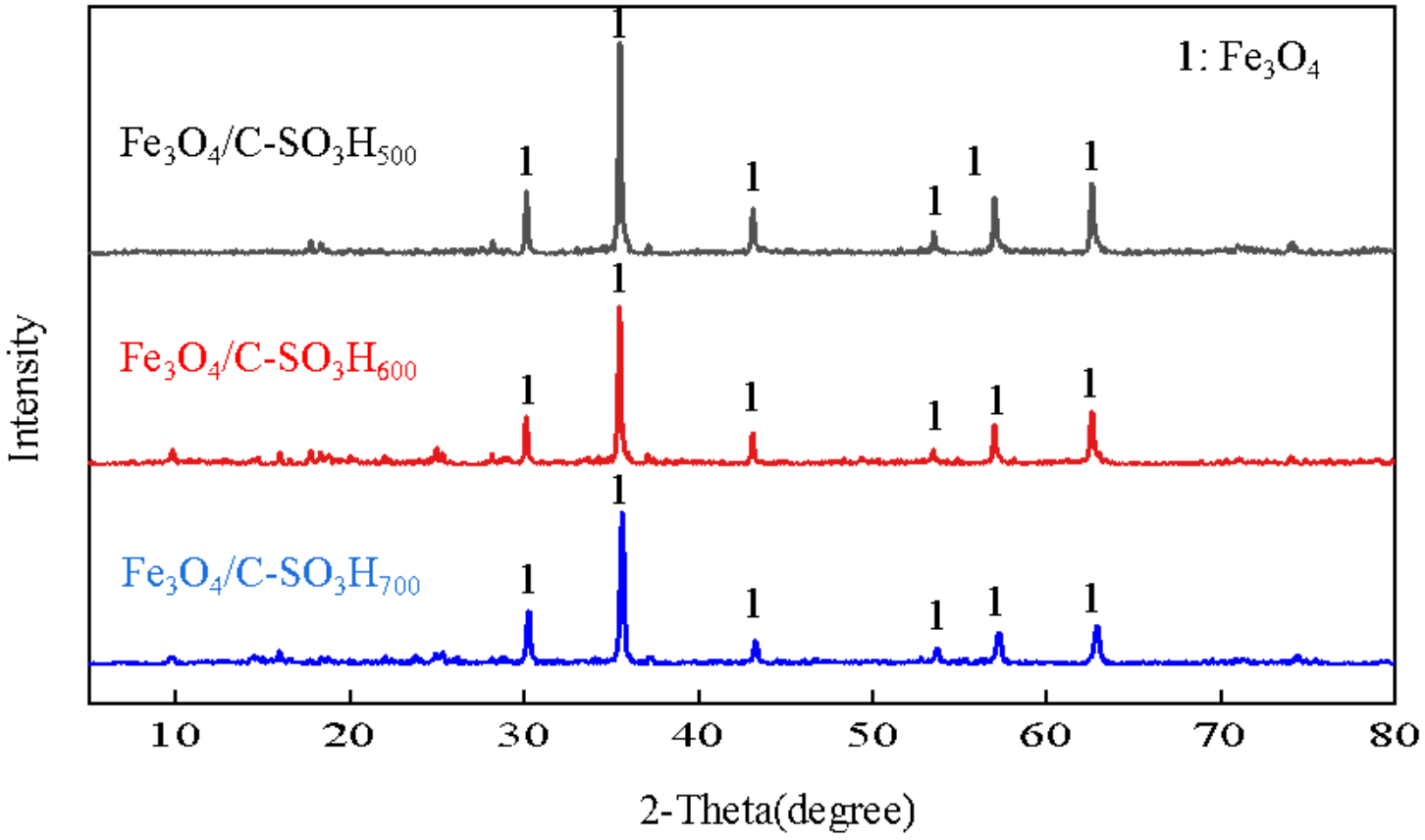

Figure 2

XRD patterns of catalysts.

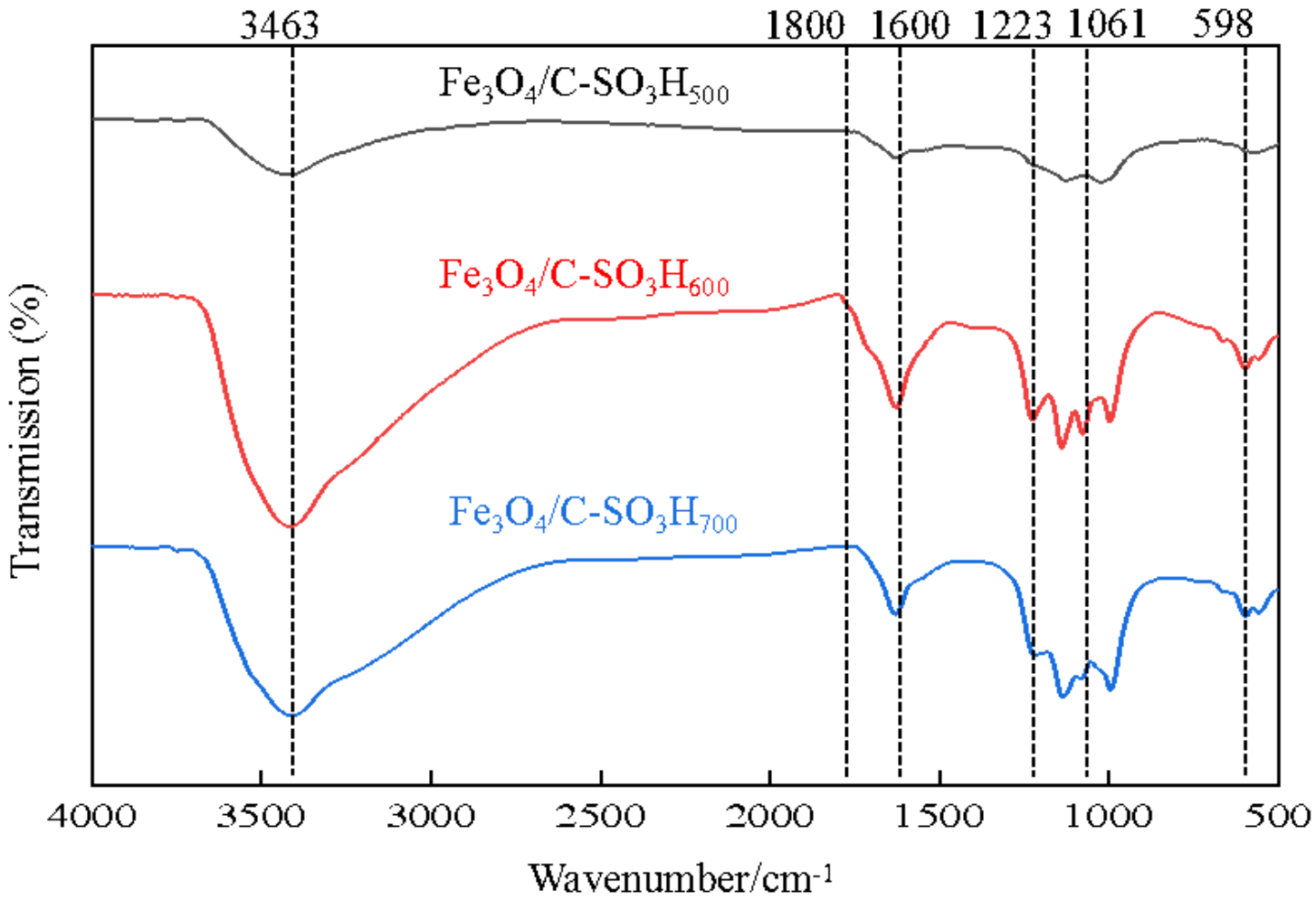

Figure 3

FTIR analysis of catalysts.

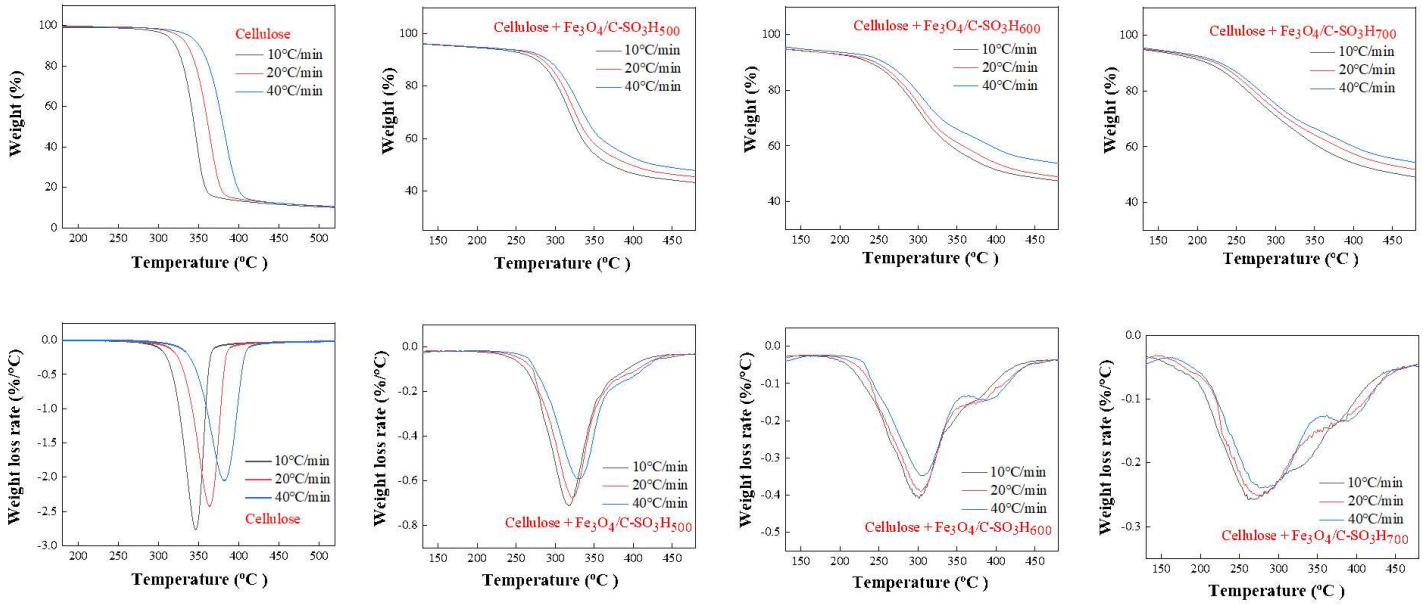

Figure 4

TG and DTG curves of cellulose and cellulose mixed with catalyst.

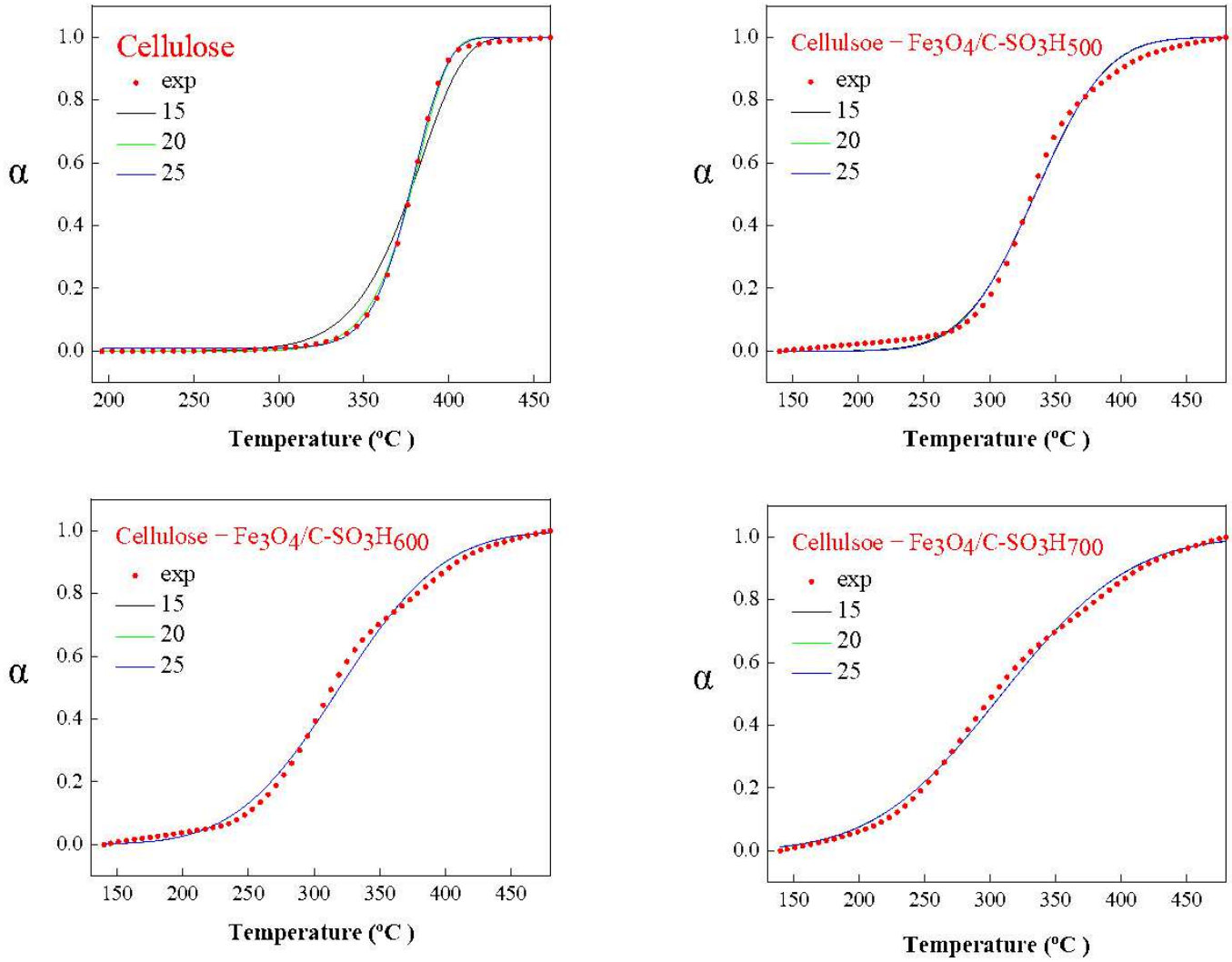

Figure 5

The experimental curve and curve fitted by DAEM model.

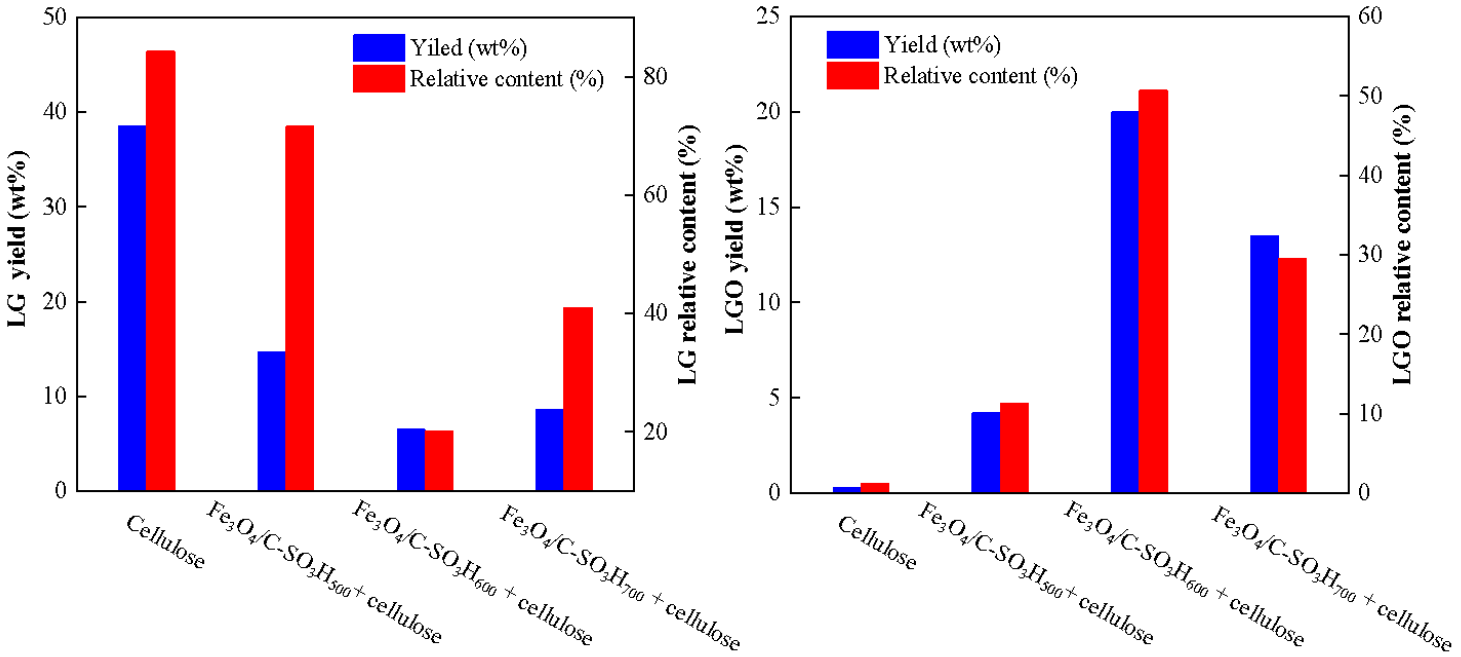

Figure 6

The effect of three catalysts to pyrolyze cellulose on the yield and relative content of LG and LGO.

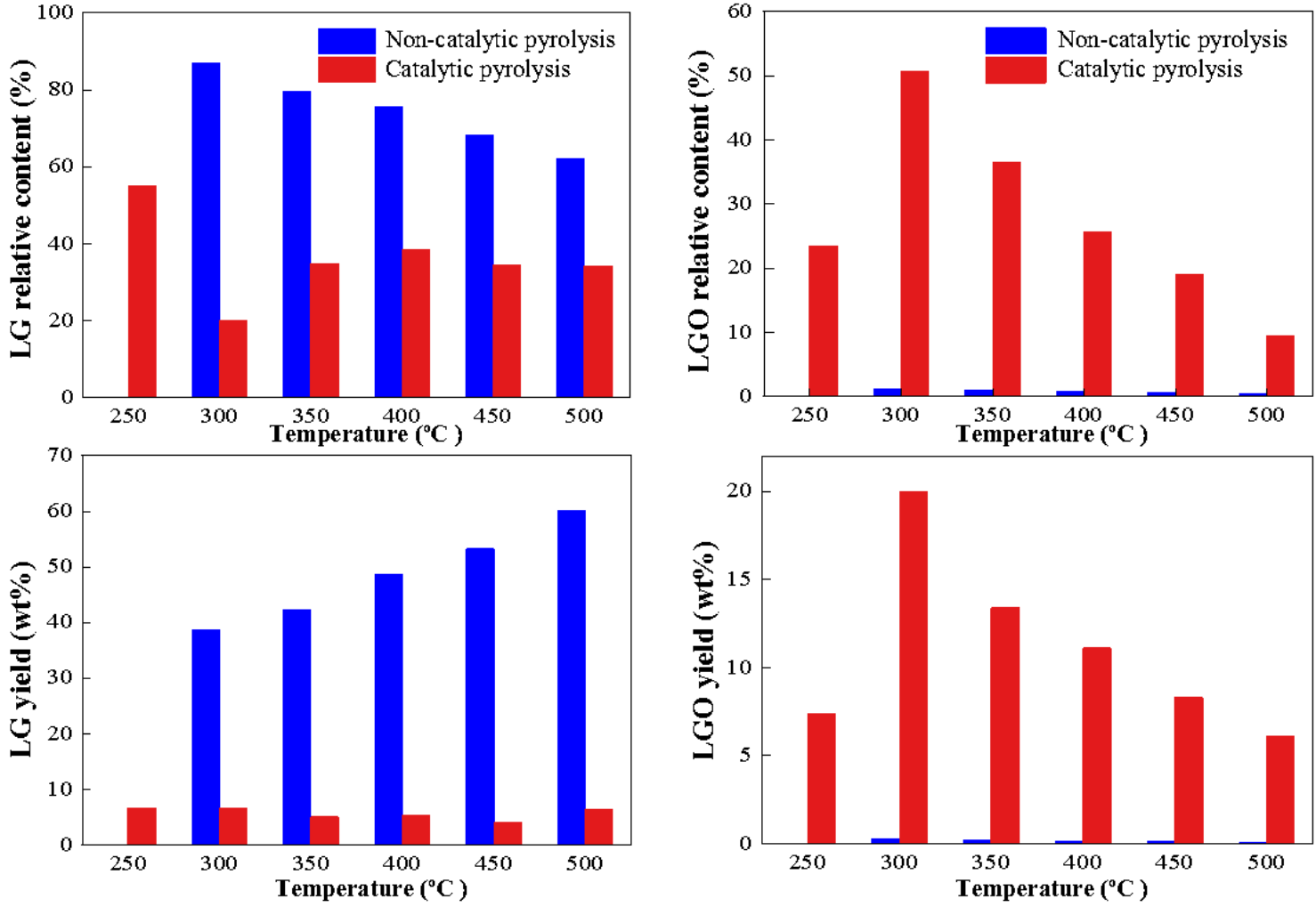

Figure 7

Effect of the temperature on the relative content and yield of LG and LGO.

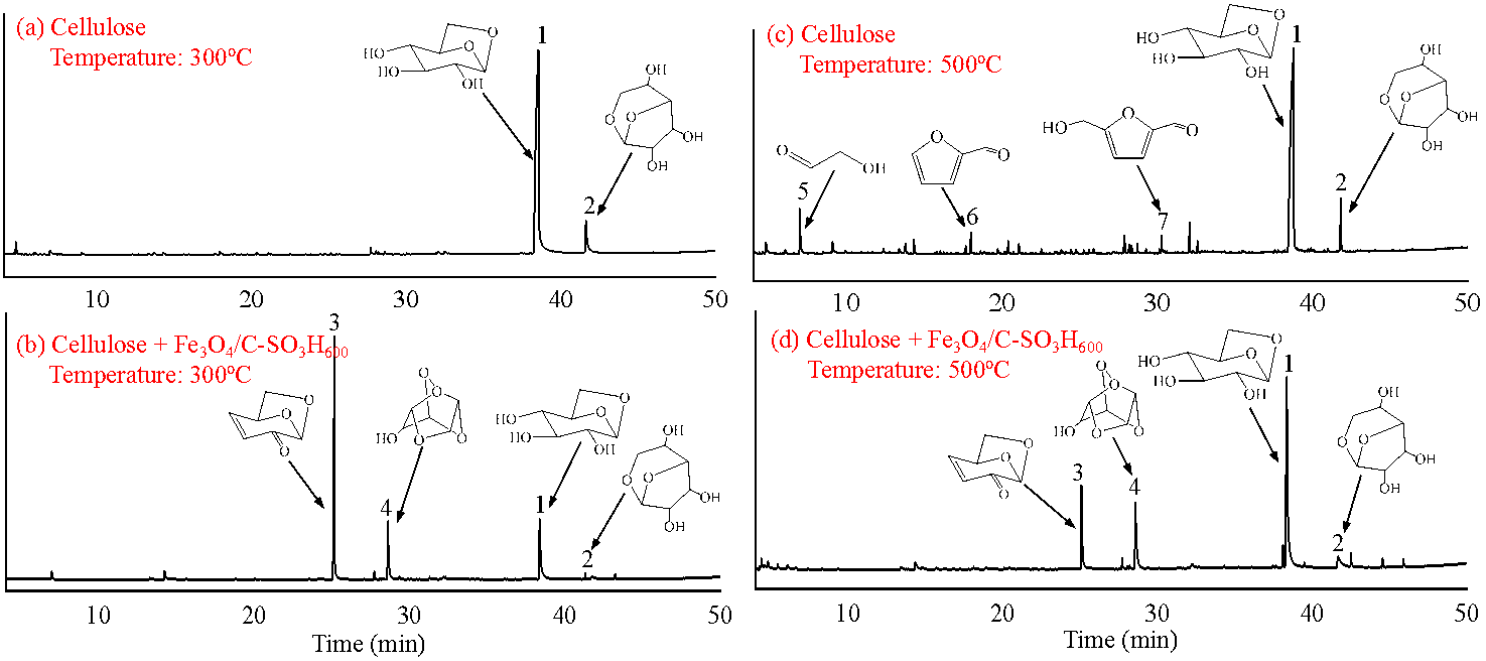

Figure 8

Typical ion chromatograms of cellulose pyrolysis: (a) cellulose in noncatalytic pyrolysis at 300 °C, (b) cellulose in catalytic pyrolysis at 300 °C, (c) cellulose in noncatalytic pyrolysis at 500 °C, (d) cellulose in catalytic pyrolysis at 500 °C, (1) LG, (2) AGF, (3) LGO, (4) DGP, (5) HAA, (6) FF, (7) 5-HMF.

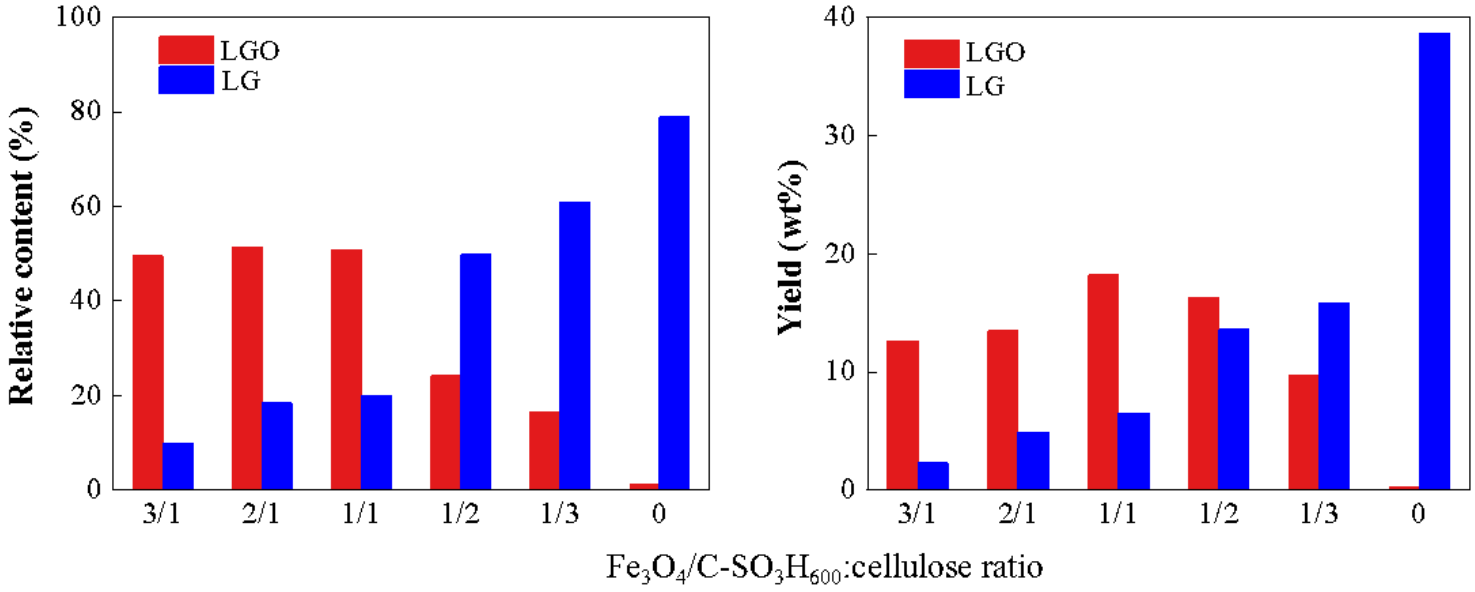

Figure 9

Effect of Fe3O4/C-SO3H600-to-cellulose ratio on the relative content and yield of LG and LGO at 300 °C.

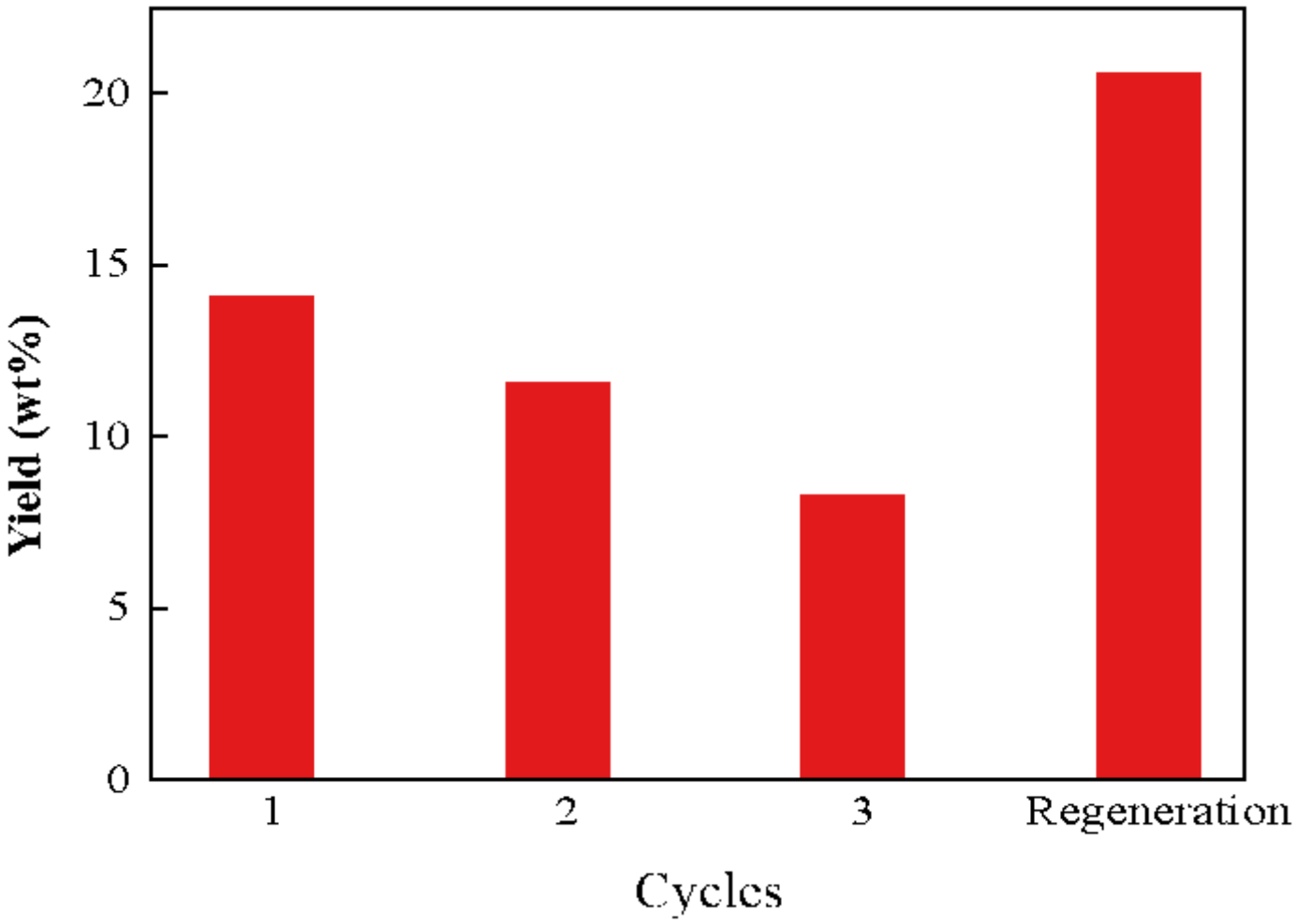

Figure 10

Effect of catalyst cycle on LGO yield at 300 °C.

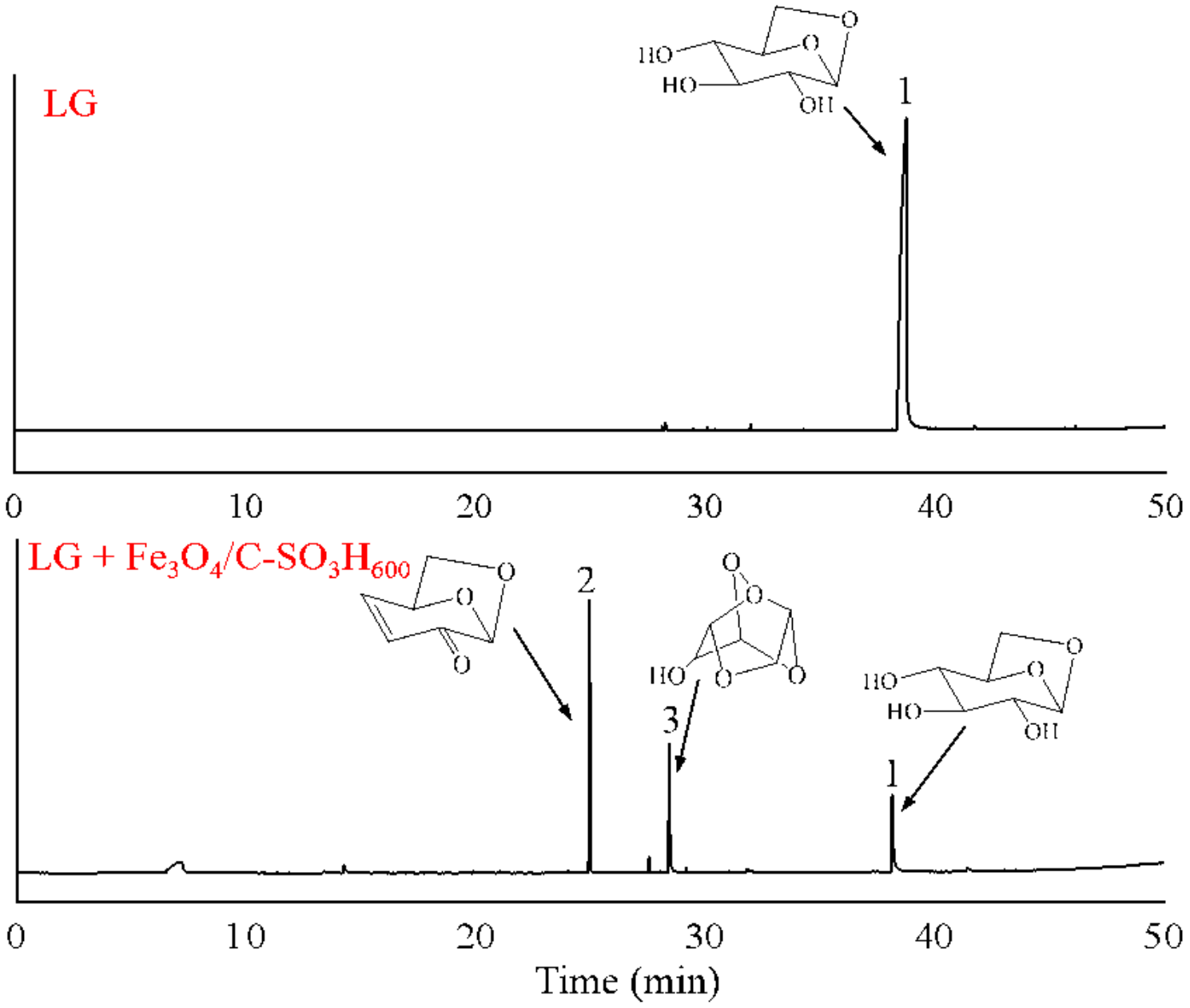

Figure 11

Typical ion chromatograms of LG in noncatalytic and catalytic pyrolysis: (1) LG, (2) LGO, (3) DGP.

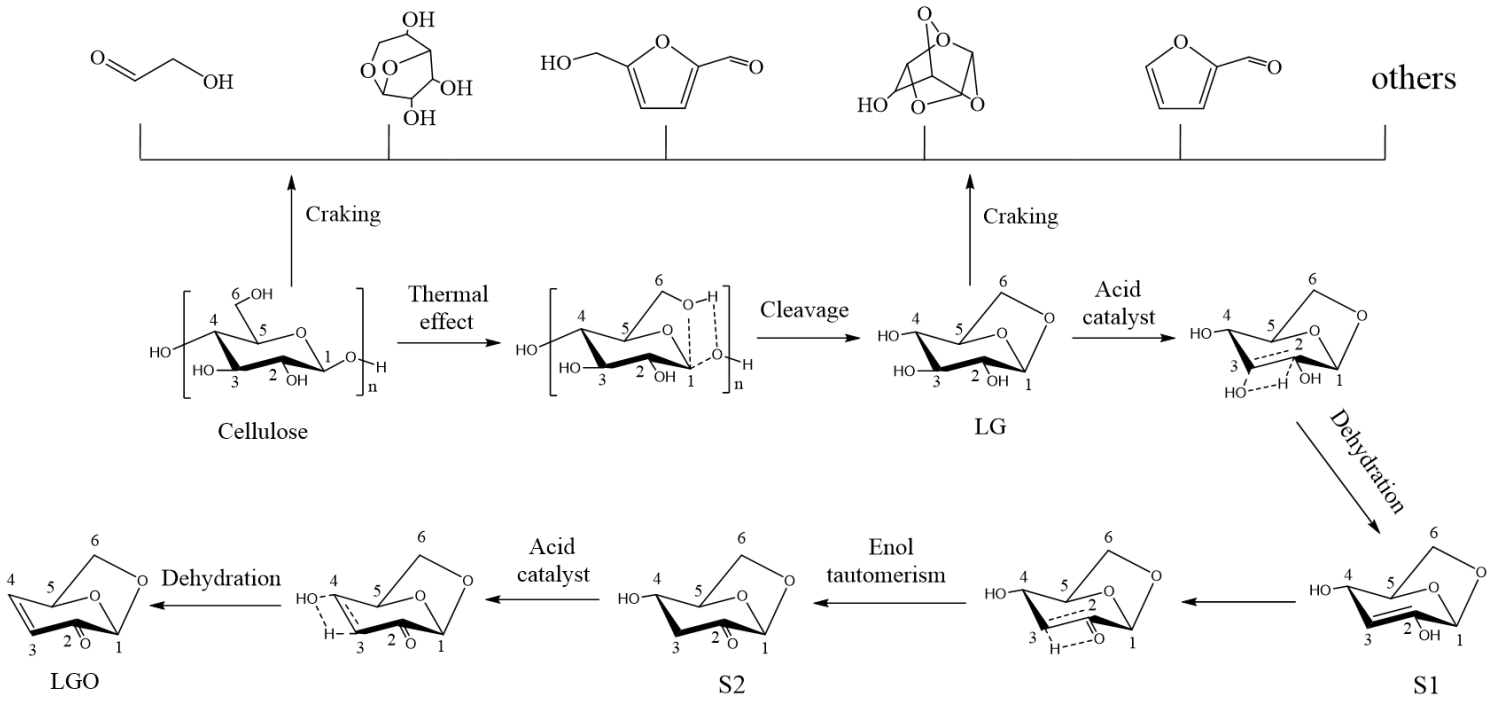

Figure 12

Possible reaction mechanism of catalytic fast pyrolysis of cellulose for LG and LGO production.